

Intrinsic behavior of face-centered-cubic supra-crystals of nanocrystals self-organized on mesoscopic scale

M. P. Pileni^{a)}

Laboratoire LM2N, Université P. et M. Curie, Paris VI, BP 52, 4 Place Jussieu, F-75231 Paris Cedex 05, France

(Received 1 August 2005; accepted 10 November 2005; published online 30 December 2005)

We describe intrinsic behavior due to the high ordering of nanocrystals at the mesoscopic scale. The first example shows well-defined columns in the formation of cobalt nanocrystals when an applied magnetic field is applied during the evaporation process. Collective breathing properties between nanocrystals are demonstrated. In both cases, these features are observed when the nanocrystals are highly ordered in fcc supra-crystals. © 2005 American Institute of Physics.

[DOI: [10.1063/1.2148368](https://doi.org/10.1063/1.2148368)]

In this paper we describe for the first time intrinsic properties due to the ordering of inorganic nanocrystals on large scale. This discovery establishes for the first time the emergence of new collective properties in three-dimensional supra-crystals. Supra-crystals are a new type of material.

I. INTRODUCTION

These last few years it has been well demonstrated,¹ due to dipolar interactions,^{1–5} that collective optical,^{1–5} magnetic,^{1,6–8} and transport^{1,9,10} properties emerge from the ordered periodic arrangement of nanocrystals in two-dimensional superlattices.

Crystals are usually atomic in origin such as the regular periodic arrangement of silicon and oxygen atoms in quartz. However they also involve larger objects such as proteins, latexes, or amorphous silica forming opal. Crystals, in fcc structure, formed by a periodic arrangement of inorganic nanocrystals having a narrow size distribution are called supra-crystals.^{11–24} They are a new and challenging area in nanotechnology.²⁵ We already know that supra-crystals are a new generation of advanced materials that are expected to exhibit unusual properties different from those of either the bulk materials or isolated nanocrystals.

We discovered that self-organization of nanocrystals in fcc supra-crystals plays a mechanical role in the control of cobalt nanocrystals organization in columns.^{26,27} An intrinsic dynamic behavior (lattice vibrations) that is absent in non-crystalline solids composed of nanoparticles is observed.^{28,29} These coherences could explain the change in the transport properties observed previously with silver nanocrystal self-organization.³⁰

II. SYNTHESIS OF NANOCRYSTALS

To highly order nanocrystals on a mesoscopic scale we demonstrate in the following that the nanocrystal self-distribution and interactions between particles and particle-

substrate are key parameters. It is necessary to control the sizes of nanocrystals composing the supra-crystals. In the following we describe these various parameters.

Our first discovery in this area was obtained 17 years ago^{31–33} by using reverse micelles as nanoreactors to control the nanoparticle size. Reverse micelles are water in oil droplets stabilized by surfactant molecules. The size of the droplet is controlled by the amount of water added. Because of the Brownian motion they collide and exchange their water content to again form two distinct micelles. These two properties permit one to produce by coprecipitation or chemical reduction nanocrystals differing by their sizes. These nanocrystals are then passivated and extracted from the micelles. At the end of the process nanocrystals coated with surfactant are produced. This procedure permits one to control the particle size and to make a very large variety of nanocrystals such as semiconductors, metal.³³ However, we have to note some limitations of this technique mainly in the shape but also time to time in the size control.³⁴ In the following we concentrate on silver and cobalt nanocrystals forming supra-crystals with intrinsic properties. In the case of silver nanoparticles³⁵ the size distribution is rather large (43%). To reduce it, a size selected precipitation process is repeated several times. At the end of the synthesis silver nanocrystals having very high crystallinity spontaneously self-organize in a compact hexagonal network.³⁶ With cobalt nanocrystals, the size distribution markedly differs with the amount of reducing agent used.³⁷ Let us define the ratio R as the reducing agent, NaBH_4 , content as $R = [\text{NaBH}_4]/[\text{Co}(\text{AOT})_2]$. The addition of a low volume of NaBH_4 , ($R < 1$) keeps stable the reverse micelles which plays the role of nanoreactors in which the nucleation and growth of cobalt nanocrystals take place. In the supersaturate regime, i.e., $R \geq 1$, micelles are destroyed because of the limiting water concentration. In such a case, two nanocrystal populations are produced. Whatever the R values are, the nanocrystals are coated with lauric acid, $\text{C}_{12}\text{H}_{25}\text{COOH}$, and then extracted from reverse micelles or from the surfactant. The TEM images obtained by deposition of a drop of solution at the end of the synthesis markedly change. At a low R value ($R=0.5$), the TEM image

^{a)}Electronic mail: pileni@sri.jussieu.fr

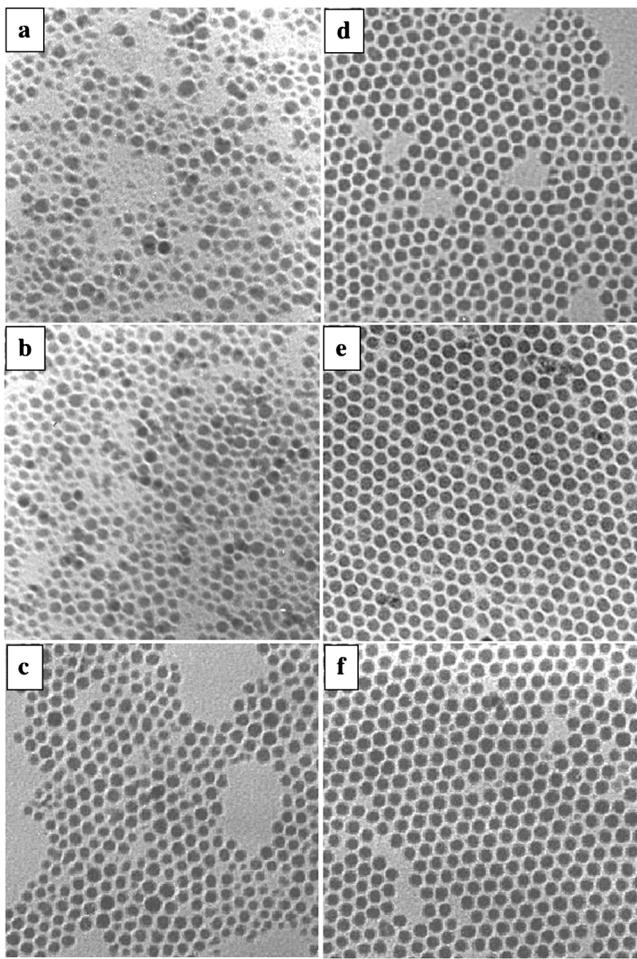


FIG. 1. TEM images of cobalt nanocrystals made at various sodium tetrahydronoboride concentrations, R . (a) $R=0.5$, (b) $R=1$, (c) $R=2$, (d) $R=4$, (e) $R=6$, and (f) $R=8$. Inset: TEM images obtained at a lower magnification.

shows nanocrystals with a local ordering. Over long distances, nanocrystals with 6 nm as average size are randomly deposited on the substrate [Fig. 1(a)]. At $R=1$, the TEM image shows almost similar behavior as that observed at $R=0.5$ [Fig. 1(b)] with an increase in the average nanocrystal size to 7 nm while there is a decrease in the size distribution (Table I). At larger R values, $R=2, 4, 6$, the average nanocrystal diameter remains the same as for $R=1$, i.e., 7 nm, while the size distribution decreases favoring the nanocrystals that self-organize in a hexagonal network [Figs. 1(c)-1(e)]. At $R=8$, the average nanocrystal diameter increases again to reach 8 nm while the size distribution further decreases [Fig. 1(f)]. The assemblies shown in Figs. 1(c)-1(f) clearly show that to obtain organizations of nanocrystals in compact hexagonal networks, the size distribution must not exceed about 13% (Table I). It has to be noted that

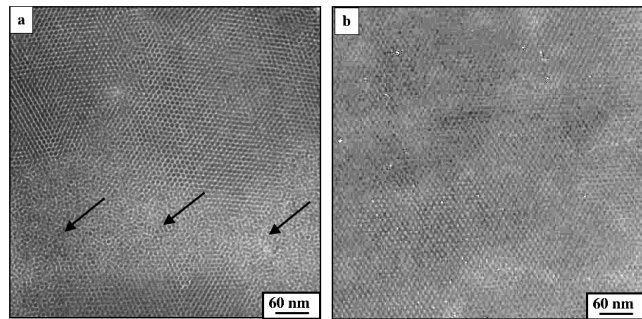


FIG. 2. TEM pattern of 7.2 nm cobalt nanocrystals organized in 3D superlattices obtained on amorphous carbon (a) and HOPG foil (b).

below this value, no change in the self-organization is observed. Drops of cobalt nanocrystals solution are deposited on an amorphous carbon coated grid for TEM examination. Figure 2(a) shows a very large coverage of nanocrystals. However, defects in the organization are observed in some parts of the TEM grid [see arrows in Fig. 2(a)]. Using highly oriented pyrolytic graphite (HOPG) as substrate leads to a better organization of the nanoparticles [Fig. 2(b)]. This confirms the fact that the nanocrystals' self-organization is obtained when their size distribution is low enough. However it also depends on the substrate that is to say the substrate-particle and particle-particle interactions. These data confirm those already obtained with silver sulfide³⁸ and silver nanocrystals.

III. CONTROL OF NANOCRYSTAL ORDERING AT THE MESOSCOPIC SCALE

To determine the influence of nanocrystal ordering on the properties of the supra-crystals, it is important to produce simultaneously ordered and disordered aggregates. By changing the substrate temperature during the deposition process of cobalt nanocrystals the ordering is tuned.³⁹ At low temperature (10°C) the deposition gives rise to the formation of a nonhomogeneous thin film coexisting with aggregates [Fig. 3(a)]. The x-ray diffraction pattern [Fig. 3(b)] reveals a broad diffuse ring attributed to an amorphous material. The peak to ring intensity ratio R_{int} characterizing the degree of preferential orientation is rather low, i.e., 1.6. On increasing the temperature ($18^{\circ}\text{C} < T < 45^{\circ}\text{C}$), the film morphology drastically changes [Figs. 3(c), 3(e), and 3(g)]. Isolated domains looking like pavements with a rather smooth surface are observed. It has to be noted that whatever the substrate temperature, the substrate coverage by nanocrystals is not homogeneous. In fact, most of the nanocrystals are deposited at the border of the substrate. On increasing the substrate temperature the pavements area increases. The x-ray diffraction patterns [Figs. 3(d), 3(f), and 3(h)] clearly show the high ordering of the nanocrystals with fcc supra-crystal formation.^{39,40} Similar behavior was observed previously with 5 nm silver nanocrystals.^{22,41} Figures 4(a) and 4(b) show the SEM and x ray patterns of 5 nm silver nanocrystals deposited at low temperature (10°C) on a substrate. This clearly indicates formation of amorphous aggregates. On increasing the substrate temperature (45°C) the

TABLE I. Average diameter of nanocrystals, D , and size distribution, σ , at various R values.

R	0.5	1	2	4	6	8
D (nm)	6	7	7	7	7	8
$\sigma\%$	30	18	13	12	12	8

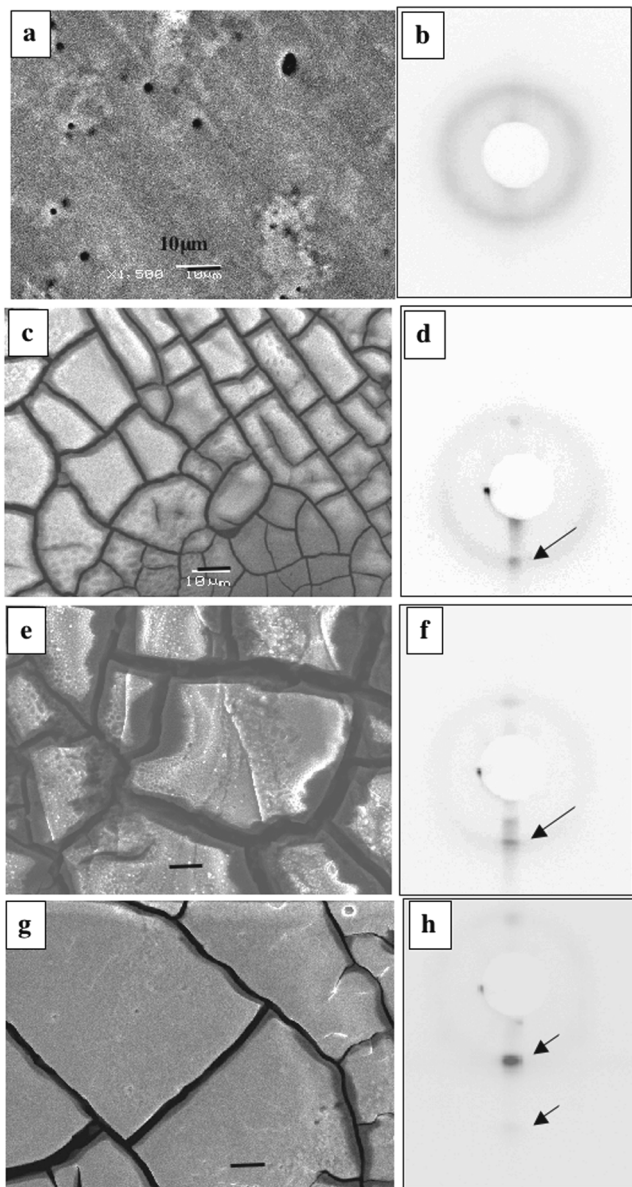


FIG. 3. SEM patterns obtained by deposition on HOPG substrate cobalt nanocrystals. The different substrate temperatures and corresponding x-ray diffraction patterns are (a),(b) $T=10\text{ }^{\circ}\text{C}$, (c),(d) $T=25\text{ }^{\circ}\text{C}$, (e),(f) $T=35\text{ }^{\circ}\text{C}$, (g),(h) $T=45\text{ }^{\circ}\text{C}$.

SEM and x-ray patterns indicate formation of fcc supracrystals [Figs. 4(c) and 4(d)]. From these data it is clearly demonstrated that it is possible to tune the ordering of nanocrystals having a low size distribution.

Instead of pavements, supra-crystals columns^{18,19} are produced by applying a magnetic field (0.25 T) perpendicular to the HOPG substrate during the evaporation process of a colloidal solution containing cobalt nanocrystals. Figure 5(a) shows a well-defined and very compact structure with columns and/or dots and very few labyrinths of cobalt nanocrystals having 5.7 nm as average diameter and 13% as size distribution. Magnifications of the patterns [insets Fig. 5(a)] show that some columns are upright whereas others have fallen. Keeping the experimental conditions similar, the HOPG substrate is replaced by a TEM grid covered with amorphous carbon. Figure 5(b) shows the TEM pattern of

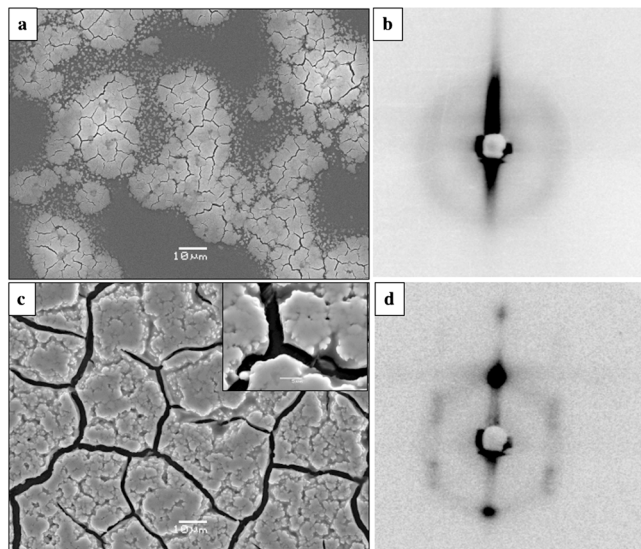


FIG. 4. SEM and x-ray diffraction patterns of 3D silver nanocrystal assemblies deposited at 10 and 22 $^{\circ}\text{C}$.

well-defined cylinders with a rather narrow size distribution are produced. The insets to Fig. 4(b) show that their extremities are made of well-ordered nanocrystals and the Fourier transform of this assembly confirmed the symmetry. From data already obtained with supra-crystals it is concluded that the cylinders are made of nanocrystals ordered in a fcc structure. On increasing the size distribution of cobalt nanocrystal to 18% keeping similar average diameter (5.9 nm) the SEM images markedly change with formation of a large number of flower-like and labyrinthine patterns [Fig. 6(a)]. Magnification of these structures shows coalescence of either upright or fallen columns forming worm-like or labyrinthine structures (insets Fig. 6). The TEM image shows finger-like structure without the appearance of organized nanocrystals. Hence by changing the size distribution of cobalt nanocrystals from 13% to 18%, the SEM and TEM patterns show formation of cylinders with a marked change in their ordering. From experiments and theoretical models, the mechanism of patterns formation in a perpendicular applied field is proposed: during the evaporation process, a liquid-gas phase transition⁴² occurs with formation of a concentrated solution of nanocrystals in equilibrium with a diluted one. In the concentrated phase, columns (dots) are progressively formed and tend to migrate. The ordering in a fcc structure of the nanocrystals, having a narrow size distribution, favors the formation of well-defined and compact columns. Because they are formed in solution they tend to diffuse and self-organize in a hexagonal network. On increasing the size distribution of nanocrystals, the interactions between particles markedly decrease and the columns are formed with disordered entities. This creates defects and the cohesive forces between columns are not large enough to keep them ordered. Columns having more or less the same sizes tend to self-assemble via van der Waals interactions, forming worm-like and labyrinthine structures. This explains the change in the height of the labyrinths. The patterns show fallen columns, earlier called

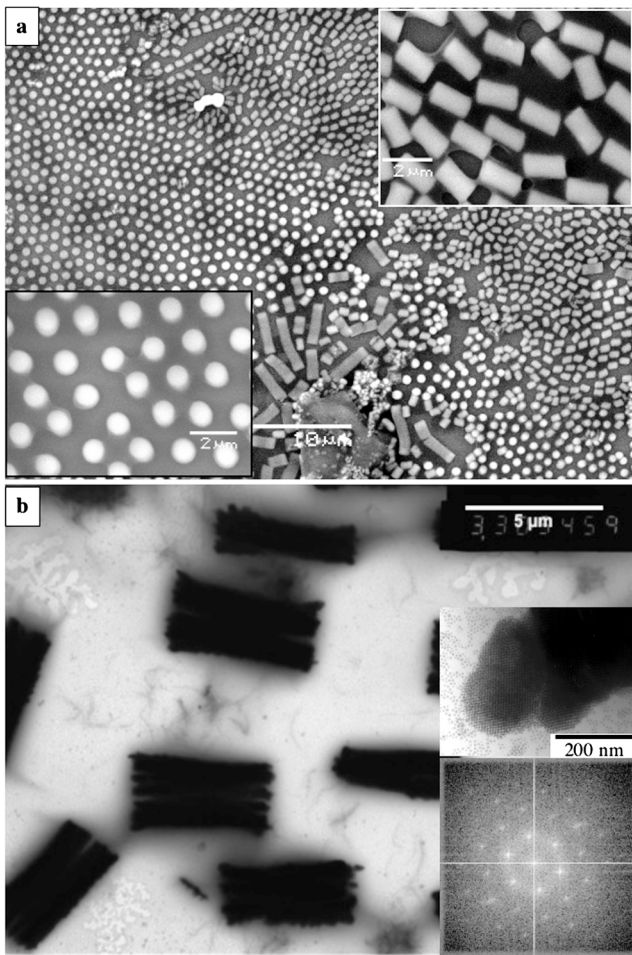


FIG. 5. SEM (a) and TEM (b) patterns of mesostructures of 5.7 nm cobalt nanocrystals having 13% as size distribution.

cylinders, because of the waves induced by capillary forces during the evaporation time.

IV. VIBRATIONAL COHERENCE INSIDE THE SUPRA-CRYSTAL

Another intrinsic property due to the self-organization of nanocrystals in fcc structure is demonstrated. When the incident light energy is in resonance with that of the electronic dipolar plasmon,⁴³ scattering by cluster vibrations is observed. For spherical nanocrystals with sizes larger than ~ 1 nm, the cluster vibrations are described by modeling the nanocrystal with a continuum nanosphere of a diameter D equal to the size of the nanocrystal,⁴⁴ and using the longitudinal, v_l , and transversal, v_t , sound velocities of bulk Ag. The vibrations are characterized by the quantum numbers n and l , and the vibrational frequencies are given by⁴⁵

$$\nu = \frac{S_{ln} \nu_t}{D}, \quad (1)$$

where S_{ln} depends on the ratio v_l/v_t . From experimentally verified group theory rules,⁴⁶ only spherical ($l=0$) and quadrupolar ($l=2$) modes are observed by low frequency Raman scattering. This was confirmed from experiments and theory considerations.⁴⁷ While the latter modes are easily detected

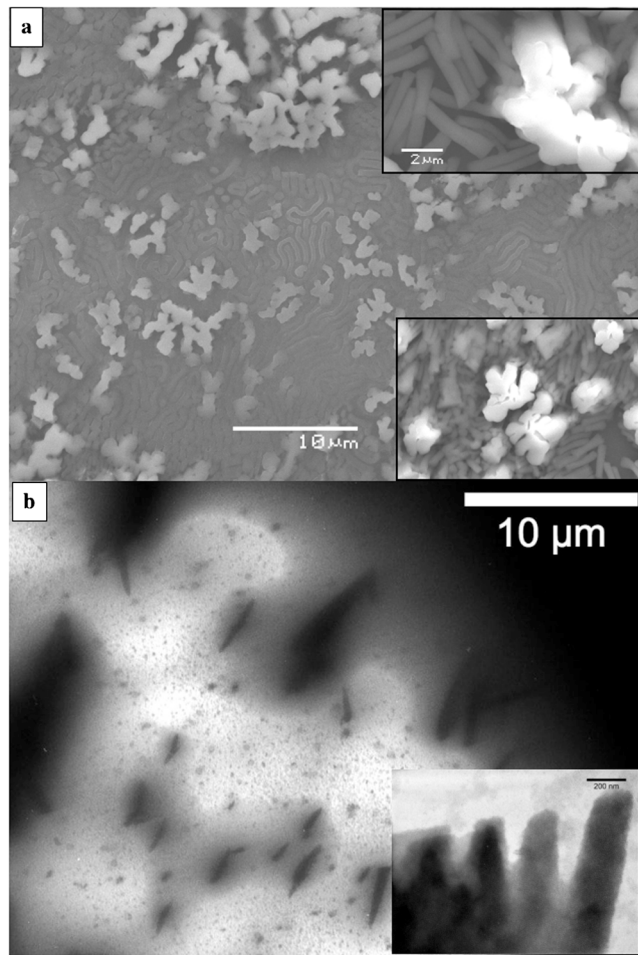


FIG. 6. SEM (a) and TEM (b) patterns of mesostructures of 5.9 nm cobalt nanocrystals having 18% as size distribution.

due to their coupling with the dipolar plasmon, the observation of the spherical modes requires a narrow size distribution of the nanocrystals.^{48–50} Solid line in Fig. 7(a) shows the HV Stokes-anti-Stokes Raman spectrum of amorphous aggregates (full line). As observed previously⁴⁴ with similar systems, the quadrupolar modes appear as sharp intense lines. Figure 8 compares the Stokes line shape of an amorphous aggregate of 5 nm silver nanocrystals with the inverse size distribution $F(D^{-1})$. From Eq. (1), a good matching of the two curves is obtained with an average sound velocity $V_t=1500$ m/s, taking $S_{ln}=0.83$, a theoretical value which corresponds to the V_l/V_t ratio of silver. Note that this sound speed value is close to that in bulk silver (1660 m/s). According to previous findings,⁴⁸ the relatively good agreement between the inverse size histogram and the Raman line shape demonstrates the *intra-nanoparticle* coherence, i.e., nanocrystallinity and not *inter-nanocrystal* coherence (or supra-crystallinity). For an isolated particle, the intensity of Raman scattering by a particle vibration changes with the degree of spatial coherence, or crystallinity, inside the Ag nanocrystals. This intensity, $I^{(1)}(\nu)$, for total *intra-nanocrystal* coherence (i.e., good nanocrystal crystallinity), without *inter-nanocrystal* coherence, is given by the following expression for Stokes-Raman scattering:⁴⁹

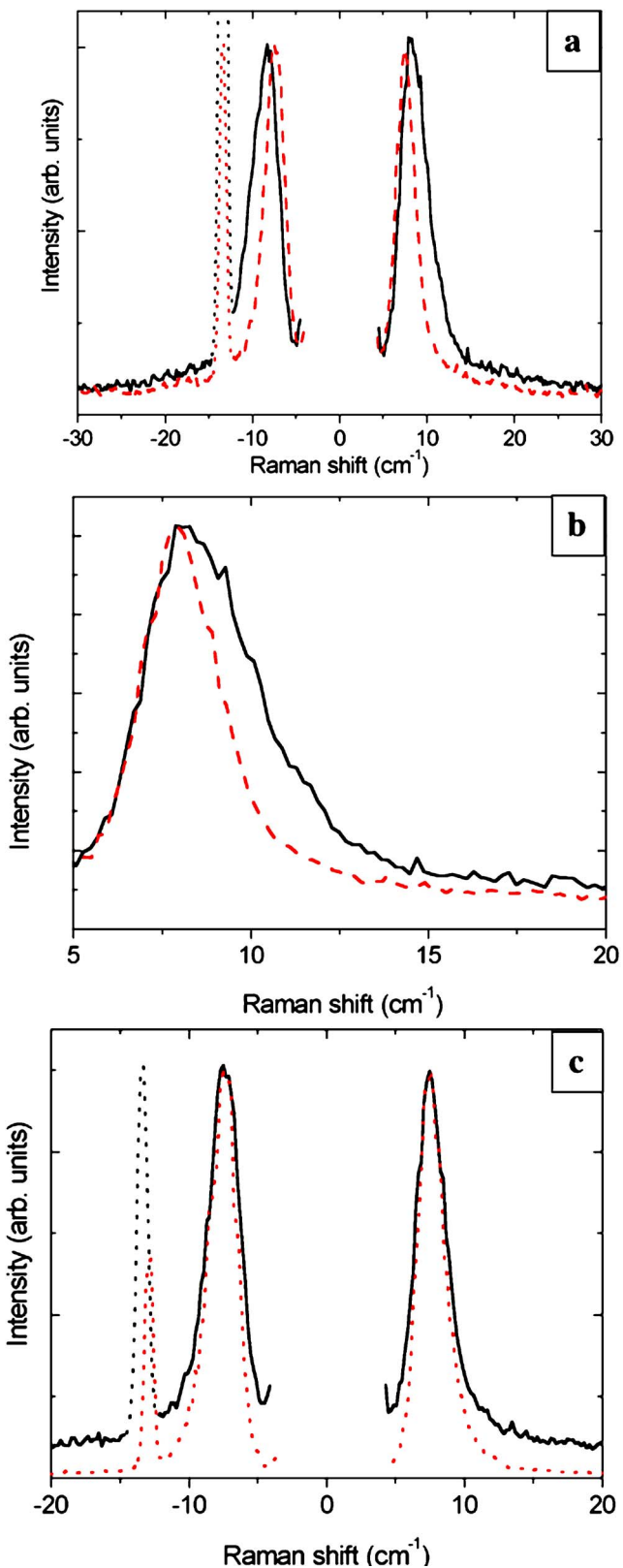


FIG. 7. (a) Raman scattering spectra of 5 nm silver nanocrystals forming either amorphous aggregates (full line) or a supra-crystal (dotted line). (b) Superposition of Stokes line shapes after horizontal shifting of amorphous aggregate and the supra-crystal. (c) Comparison of the Raman scattered intensity $I^{(3)}(\nu)$ from silver nanocrystals forming small supra-crystals with the profile $[I^{(1)}(\nu)]^2$ from amorphous aggregate of silver nanocrystals.

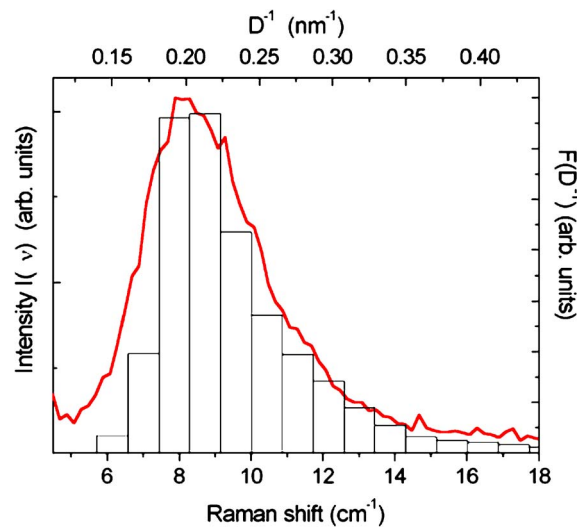


FIG. 8. Comparison of the Stokes line shapes of amorphous aggregates.

$$I^{(1)}(\alpha) = \frac{n(\alpha) + 1}{\alpha} [\alpha^{(1)} \delta(\delta)] F(\alpha), \quad (2)$$

where $n(n)$ is the Bose factor, $\delta^{(1)} \delta(\delta)$ the polarizability fluctuation of an isolated nanocrystal, and $F(\nu)$ is the normalized frequency distribution, which is related to the normalized inverse size distribution, $F(D^{-1})$, through Eq. (1) ($F(\nu)d\nu = F(D^{-1})dD^{-1}$). Obviously, $\delta^{(1)} \delta(\delta)$ is proportional to the number of atoms, N_D , in a nanocrystal when there is *intrananocrystal* coherence. Because of the frequency dependence of the different terms in Eq. (2), the scattering intensity of an assembly of nanocrystals is proportional to the frequency distribution:

$$I^{(1)}(\infty) \propto F(\infty). \quad (3)$$

Such proportionality is verified with disordered aggregates (Fig. 8).

In the present paper we want to demonstrate that internanocrystal coherence takes place when the 5 nm silver nanocrystals are highly ordered in fcc supra-crystals.^{28,29,51} Figure 7(a) compares the HV Raman spectra of amorphous aggregate and supra-crystals. The Raman peak corresponding to the supra-crystal quadrupolar modes is shifted toward a low frequency compared to the amorphous aggregate Raman peak with a decrease of its width [Fig. 7(b)]. The narrowing of the Raman quadrupolar peak is only visible for the small supra-crystals. To explain this change in the behavior with the ordering of nanocrystals two effects have to be taken into account: the effect of the Lorentz field and that of vibrational coherence in a supra-crystal: (i) *Effect of the Lorentz field*. The electromagnetic field, which is induced on each nanocrystal by the (vibration-fluctuating) electric dipoles of the neighboring nanocrystals organized in fcc supra-crystals, changes the nanocrystal polarizability fluctuation, $\alpha \alpha(\alpha)$. This effect exists if the electromagnetic fields induced by the different neighboring nanocrystals are in phase. Consequently, the electromagnetic coherence is necessary for this effect, as it occurs with the supracrystalline arrangements. In this case, the nanocrystal polarizability fluctuation,

$\alpha\alpha(\alpha)$, in a supra-crystal, is equal to the polarizability fluctuation of an isolated nanocrystal, $\delta^{(1)}\delta(\delta)$, multiplied by the factor $L(\nu)$, that accounts for the Lorentz field. $L(\nu)$ is dependent on the size D of the nanocrystals in the supra-crystal, and thus on ν through Eq. (1): $\delta\delta(\delta)=L(\delta)\delta^{(1)}\delta(\delta)$. (ii) *Effect of vibrational coherence.* The vibrational coherence among the nanocrystals in a supra-crystal is established due to the weak interdigitization of the thiol chains. The van der Waals bonding between thiol chains is too weak to have a measurable effect on the vibrational frequencies of nanocrystals. However it is sufficient to establish a correlation between the vibrating nanocrystals, so that they vibrate coherently in a supra-crystal. The quadrupolar modes in a supra-crystal are like nondispersive optical modes. For small (size $\leq 1/10$, 1 being the light wavelength) supra-crystals, the light is scattered by stationary modes in the supra-crystal, like by the vibration modes in a molecule. In Raman light scattering, the vibration modes are regarded as localized, so that momentum conservation has no need to be considered explicitly. In other words, the Raman-active modes are determined only by their symmetry. The effective supra-crystal polarizability fluctuation at the frequency n is equal to the nanocrystal polarizability fluctuation $\alpha\alpha(\alpha)$, multiplied by the number N_{SD} of nanocrystals both in the supra-crystal. Therefore, from above, the intensity of Raman scattering from a supra-crystal containing N_{SD} nanocrystals is proportional to $[N_{SD}L(\delta)\delta^{(1)}\delta(\delta)]$. In consequence, the intensity of Raman scattering from a sample organized into small supra-crystals is expressed as follows:²⁹

$$I^{(3)}(\infty) \propto L^2(\infty)[I^{(1)}(\infty)]^2. \quad (4)$$

The Stokes and anti-Stokes $I^2(n)$ profiles were horizontally shifted and vertically rescaled for the peak maxima to match. The line profile is given by the square of that corresponding to a disordered arrangement of nanocrystals. This is illustrated by Fig. 7(c): the narrowed peak of the “small” supra-crystals has the same profile as the square of the non-narrowed peak of the “disordered” aggregate.

V. CONCLUSIONS

In the present paper we demonstrate that manipulation of nanocrystals having a narrow size distribution permits one to build regular arrangement of nanometer scale spheres at mesoscopic scale. These supra-crystals, characterized by fcc structure, are a new class of materials. Of particular interest is the question of whether new collective properties emerge from the ordered periodic arrangement of nanocrystals in supra-crystals. We discovered that self-organization of nanocrystals in fcc supra-crystals plays a mechanical role in the control of cobalt nanocrystal organization in columns. An intrinsic dynamic behavior (lattice vibrations) that is absent in noncrystalline solids composed of nanoparticles is observed. According to News and Views in Nature Materials,³ the importance of this discovery establishes for the first time the emergence of a new collective property in three-dimensional (3D) supra-crystals.

- ¹M. P. Pilani, J. Phys. Chem. B **105**, 3358 (2001).
- ²A. Taleb, C. Petit, and M. P. Pilani, J. Phys. Chem. B **102**, 2214 (1998).
- ³N. Pinna, M. Maillard, A. Courty, V. Russier, and M. P. Pilani, Phys. Rev. B **66**, 45415 (2002).
- ⁴M. Maillard, P. Monchicourt, and M. P. Pilani, Chem. Phys. Lett. **107**, 7492 (2003).
- ⁵N. Nilius, H.-M. Benia, C. Salzemann, H.-J. Freund, A. Brioude, and M.-P. Pilani, Chem. Phys. Lett. (in press).
- ⁶C. Petit, A. Taleb, and M. P. Pilani, Adv. Mater. (Weinheim, Ger.) **10**, 259 (1998).
- ⁷C. B. Sun, D. Murray, L. Weller, A. Folks, and A. Moser, Science **287**, 1989 (2000).
- ⁸V. Russier, C. Petit, and M. P. Pilani, J. Appl. Phys. **93**, 10001 (2003).
- ⁹G. Markovich, C. P. Collier, and J. R. Heath, Phys. Rev. Lett. **80**, 3807 (1998).
- ¹⁰A. Taleb, F. Silly, A. O. Gusev, F. Charra, and M. P. Pilani, Adv. Mater. (Weinheim, Ger.) **12**, 633 (2000).
- ¹¹L. Motte, F. Billoudet, and M. P. Pilani, J. Phys. Chem. **99**, 16425 (1995).
- ¹²C. B. Murray, C. R. Kagan, and M. G. Bawendi, Science **270**, 1335 (1995).
- ¹³M. Brust, D. Bethell, D. J. Schiffrin, and C. Kiely, Adv. Mater. (Weinheim, Ger.) **9**, 797 (1995).
- ¹⁴S. A. Harfenist, Z. L. Wang, M. M. Alvarez, I. Vezmar, and R. L. Whetten, J. Phys. Chem. **100**, 13904 (1996); L. Motte, F. Billoudet, E. Lacaze, and M. P. Pilani, Adv. Mater. (Weinheim, Ger.) **8**, 1018 (1996).
- ¹⁵R. L. Whetten, J. T. Khoury, M. M. Alvarez, S. Murthy, I. Vezmar, Z. L. Wang, C. C. Cleveland, W. D. Luedtke, and U. Landman, Adv. Mater. (Weinheim, Ger.) **8**, 428 (1996).
- ¹⁶S. A. Harfenist, Z. L. Wang, M. M. Alvarez, I. Vezmar, and R. L. Whetten, J. Phys. Chem. **100**, 13904 (1996).
- ¹⁷S. Murthy, Z. L. Wang, and R. L. Whetten, Philos. Mag. Lett. **75**, 321 (1997).
- ¹⁸L. Motte, F. Billoudet, J. Douin, E. Lacaze, and M. P. Pilani, J. Phys. Chem. **101**, 138 (1997).
- ¹⁹L. Motte and M. P. Pilani, J. Phys. Chem. **102**, 4104 (1998).
- ²⁰B. A. Korgel, S. Fullam, S. Connolly, and D. Fitzmaurice, J. Phys. Chem. **8379**, 102 (1998).
- ²¹B. A. Korgel and D. Fitzmaurice, Phys. Rev. B **59**, 14191 (1999).
- ²²A. Courty, C. Fermon, and M. P. Pilani, Adv. Mater. (Weinheim, Ger.) **13**, 254 (2001).
- ²³I. Lisiecki, P. A. Albouy, and M. P. Pilani, Adv. Mater. (Weinheim, Ger.) **15**, 712 (2003).
- ²⁴I. Lisiecki, P. A. Albouy, and M. P. Pilani, J. Phys. Chem. B **108**, 20050 (2004).
- ²⁵M. Brust, Nat. Mater. **4**, 354 (2005).
- ²⁶V. Germain, and M. P. Pilani, Adv. Mater. (Weinheim, Ger.) **17**, 1424 (2005).
- ²⁷V. Germain and M. P. Pilani, J. Phys. Chem. **109**, 5548 (2005).
- ²⁸A. Courty, A. Merme, P. A. Albouy, E. Duval, and M. P. Pilani, Nat. Mater. **4**, 395 (2005).
- ²⁹E. Duval, A. Merme, A. Courty, P. A. Albouy, and M. P. Pilani, Phys. Rev. B **72**, 85439 (2005).
- ³⁰A. Taleb, F. Silly, A. O. Gusev, F. Charra, and M. P. Pilani, Adv. Mater. (Weinheim, Ger.) **12**, 633 (2000).
- ³¹P. Petit and M. P. Pilani, J. Phys. Chem. **92**, 2282 (1988).
- ³²M. P. Pilani, J. Phys. Chem. **97**, 6961 (1993).
- ³³M. P. Pilani, Langmuir **13**, 3266 (1997).
- ³⁴M. P. Pilani, Nat. Mater. **2**, 141 (2003).
- ³⁵P. Petit, P. Lixon, and M. P. Pilani, J. Phys. Chem. **97**, 12974 (1993).
- ³⁶A. Taleb, C. Petit, and M. P. Pilani, Chem. Mater. **9**, 950 (1997).
- ³⁷I. Lisiecki and M. P. Pilani, Langmuir **19**, 9486 (2003).
- ³⁸L. Motte, E. Lacaze, M. Maillard, and M. P. Pilani, Langmuir **16**, 3803 (2000).
- ³⁹I. Lisiecki, P. A. Albouy, and C. Pilani, J. Phys. Chem. **108**, 20050 (2004).
- ⁴⁰I. Lisiecki, P. A. Albouy, and M. P. Pilani, J. Adv. Mater. **15**, 712 (2003).
- ⁴¹A. Courty, O. Araspin, C. Fermon, and M. P. Pilani, Langmuir **17**, 1372 (2001).
- ⁴²V. Germain, J. Richardi, D. Ingert, and M. P. Pilani, J. Phys. Chem. B (in press).
- ⁴³B. Palpant, H. Portales, L. Saviot, J. Lermé, B. Prével, M. Pellarin, E. Duval, A. Perez, and M. Broyer, Phys. Rev. B **60**, 17107 (1999).
- ⁴⁴E. Duval, A. Boukenter, and B. Champagnon, Phys. Rev. Lett. **56**, 2052 (1986).
- ⁴⁵H. Lamb, Proc. London Math. Soc. **13**, 189 (1882).

⁴⁶E. Duval, Phys. Rev. B **46**, 5795 (1992).

⁴⁷M. Fujii, T. Nagareda, S. Hayashi, and K. Yamamoto, Phys. Rev. B **44**, 6243 (1991).

⁴⁸H. Portales, L. Saviot, E. Duval, M. Fujii, S. Hayashi, N. Del Fatti, and F. Vallée, J. Chem. Phys. **115**, 3444 (2001).

⁴⁹E. Duval, H. Portales, L. Saviot, M. Fujii, K. Sumitomo, and S. Hayashi, Phys. Rev. B **63**, 075405 (2001).

⁵⁰A. Courty, I. Lisiecki, and M. P. Pilani, J. Chem. Phys. **116**, 8074 (2002).

⁵¹A. Courty, P. A. Albouy, E. Duval, A. Mermet, and M. P. Pilani, J. Phys. Chem. B **109**, 21159 (2005).